ELSEVIER

Comput. Methods Appl. Mech. Engrg. 182 (2000) 217–245

Computer methods in applied mechanics and engineering

www.elsevier.com/locate/cma

The *TRIC* shell element: theoretical and numerical investigation

J.H. Argyris [a], M. Papadrakakis [b,*], C. Apostolopoulou [b], S. Koutsourelakis [b]

[a] *Institute for Computer Applications, Pfaffenwaldring 27, University of Stuttgart, D-70569 Stuttgart, Germany*
[b] *Institute of Structural Analysis and Seismic Research, National Technical University of Athens, Athens 15773, Greece*

Received 13 January 1999

Abstract

The TRIC facet triangular shell element, which is based on the natural mode method, is seen under the light of the non-consistent formulation proposed by Bergan and co-workers. Under this formulation, the convergence requirements are fulfilled even with relaxed conditions on the conformity demands of the displacement shape functions. The intrinsic connection between the non-consistent formulation and the natural mode method is demonstrated, establishing thus a rigorous theoretical foundation for the TRIC element. Under the perspective of the non-consistent formulation, TRIC's convergence characteristics are established by satisfying apriori the patch test due to its inherent properties and thus guaranteeing convergence to the exact solution. Furthermore, the element's accuracy, robustness and efficiency are tested in a number of judiciously selected numerical examples on benchmark plate and shell problems, while a CPU time comparison with a pure displacement-based isoparametric shell element demonstrates its computational merits.

1. Introduction

Finite element analysis of shells has been receiving continuous attention since the early days of the development of the method. The analysis of shells presents a challenge, since their formulation may become cumbersome and their behaviour can be unpredictable with regard to geometry or support conditions. The pure displacement-based isoparametric formulation suffers from various kinds of locking phenomena, which are only partially dealt with by reduced or selective integration techniques. Ongoing research efforts have been focused on devising more elaborate element models that circumvent the deficiencies of the pure-displacement elements. Thus, a number of approaches have been proposed based on mixed or hybrid formulations, incompatible displacement methods, stabilization methods, assumed strain methods and free formulations.

An attempt to device a shell element with robustness, accuracy and efficiency has led to the derivation of the TRIC shell element [1,2], a simple but sophisticated triangular, shear-deformable facet shell element suitable for the analysis of thin and moderately thick isotropic as well as composite plate and shell structures. Its formulation is based on the natural mode finite element method [3], a method introduced by Argyris in the late 1960s that separates the pure deformational modes – also called natural modes – from the rigid body movements of the element. The natural mode method has substantial computational advantages compared to the conventional isoparametric finite element formulations, since it eliminates the costly numerical integration by deriving stiffness matrices with simple algebraic expressions. On the other

* Corresponding author. Fax: +301-7721693.
E-mail address: mpapadra@central.ntua.gr (M. Papadrakakis).

0045-7825/00/$ - see front matter
PII: S0045-7825(99)00094-8

hand, the inclusion of the transverse shear deformations in the formulation of the TRIC shell element is performed in a way that eliminates the shear locking effect in a physical manner, based on a first-order shear deformable beam theory.

The derivation of TRIC's stiffness matrix was established upon a rather physical approach based on the observation of the element's deformational modes and the accumulated experience of Argyris and co-workers obtained from previous shell elements that they have developed using physical lumping procedures. In Ref. [1], the formulation of TRIC is presented as an evolution step emerging from three previous elements, namely TRUMP [4], TRUNC [5] and LACOT [6]. This approach, however, which deviates from standard finite element formulations, may give rise to doubts concerning the theoretical justification of some of the steps taken. As seen in Ref. [1], the shape functions used for the interpolation of the displacement field are assumed to be non-conforming, while the coupling terms between the symmetric and antisymmetric modes in the natural stiffness matrix are set equal to zero. The main goal of this paper is to provide a more rigorous mathematical foundation for the derivation of TRIC shell element and to show that the element, due to its inherent properties, guarantees convergence to the exact solution. This is done by setting TRIC under the light of the non-consistent formulation [7].

In the late 1970s, Bergan and co-workers [8,9] started investigating the relationship between the convergence characteristics of a finite element and the conformity of the shape functions in the assumed displacement field. The results of this research showed that interelement continuity appeared not to be an obstacle to convergence provided that the shape functions used in connection with the potential energy principle are energy and force orthogonal. Bergan and Nygard [7], proceeded further in relaxing the above requirements of orthogonality and suggested two alternative formulations, the non-consistent one where only the force orthogonality condition is satisfied and the free formulation where the only requirement set is that the displacement patterns used should be linearly independent. In a more recent work, Felippa et al. [10] presented a comprehensive formulation of parametrized element families using the concept of finite element templates, which represent element-level stiffness equations containing free parameters. All these finite element formulations guarantee convergence in the sense that the derived stiffness matrices satisfy a set of linear constraints imposed by Iron's patch test on an element level, or else the so-called individual element test. The basis for these formulations is that the interpolation of the cartesian displacement field is done in terms of generalized displacement patterns rather than nodal displacements. The shape functions are partitioned in two distinct components: one of them associated to rigid body-constant strain modes and the other to higher order modes.

It appears that there is an intrinsic connection of the aforementioned formulations to the natural mode method according to which the deformation modes are separated to rigid body and to pure natural deformational patterns. It will be shown that the TRIC shell element satisfies the individual element test and according to the non-consistent formulation its use guarantees convergence. On the other hand, significant advantages of the element, such as the incorporation of the transverse shear deformations in a way that defies the shear-locking phenomenon, will be discussed in detail. A complete presentation is therefore attempted, establishing a rigorous theoretical formulation for the element. Furthermore, the element's robustness and accuracy will be shown in a variety of judiciously selected test examples for a set of plate and shell problems, while its computational efficiency will be demonstrated by comparing the CPU performance of the element with the 8-node serendipity shell element.

2. Finite element formulations with increased freedom in choosing shape functions

In this section, the finite element formulations proposed by Bergan and co-workers will be reviewed in an attempt to help the reader understand the immediate connection to the natural mode method and the formulation of the TRIC element.

2.1. The individual element test

The principle virtue of the patch test is that, if an element passes the test, then the finite element solution will converge toward the correct solution for successive mesh refinements. The core of this test is that a

patch of elements should be capable of reproducing an arbitrary state of constant strain identically as the mesh becomes finer or else as the element size goes towards zero. It is obvious that the patch test is not directly applicable to a single element. Bergan and Hanssen [9], however, contrived an equivalent test, called the individual element test, which is applicable to a single element and plays an integral role in the development of finite element formulations with increased freedom in choosing shape functions. According to the individual element test, convergence is guaranteed if a single element, when interacting with its neighbours, is capable of identically modelling an arbitrary state of constant strain, or else if the element stiffness matrix produces the exact sum of connecting forces computed from lumped tractions during arbitrary constant strain field. This test is in fact a set of linear constraint equations that apply directly to the element's stiffness matrix.

Following the notation introduced by Bergan, let the displacement field over the region of an element be expressed as:

$$u = \begin{bmatrix} N_{\mathrm{rc}} & N_{\mathrm{h}} \end{bmatrix} \begin{bmatrix} q_{\mathrm{rc}} \\ q_{\mathrm{h}} \end{bmatrix} = Nq, \tag{1}$$

where N_{rc} and N_{h} represent a complete set of linearly independent shape functions associated to rigid body-constant strain and higher order modes, respectively, while q_{rc} and q_{h} are the corresponding coefficients otherwise called generalized modes or generalized degrees of freedom. The total number of rc- and h-modes should be equal to n_{t}, which is the total number of the degrees of freedom of the element.

$$n_{\mathrm{t}} = n_{\mathrm{rc}} + n_{\mathrm{h}}. \tag{2}$$

The strain field over the element region is then expressed via

$$\varepsilon = \begin{bmatrix} B_{\mathrm{rc}} & B_{\mathrm{h}} \end{bmatrix} \begin{bmatrix} q_{\mathrm{rc}} \\ q_{\mathrm{h}} \end{bmatrix} = B_q\, q, \tag{3}$$

where B_{rc} and B_{h} contain gradients of the generalized shape functions. The expression for the stress field is given by

$$\sigma = C\,\varepsilon = C B_q\ q, \tag{4}$$

where C denotes the constitutive matrix of the element. The relationship between the nodal degrees of freedom v and the generalized degrees of freedom q can easily be obtained by substituting the nodal coordinates in Eq. (1)

$$v = \underset{(n_{\mathrm{t}} \times n_{\mathrm{t}})}{\begin{bmatrix} G_{\mathrm{rc}} & G_{\mathrm{h}} \\ (n_{\mathrm{t}} \times n_{\mathrm{rc}}) & (n_{\mathrm{t}} \times n_{\mathrm{h}}) \end{bmatrix}} \begin{bmatrix} q_{\mathrm{rc}} \\ q_{\mathrm{h}} \end{bmatrix} = \underset{(n_{\mathrm{t}} \times n_{\mathrm{t}})}{G}\, q. \tag{5}$$

When a patch of elements is under the effect of a rigid body motion and a constant strain state ($q_{\mathrm{h}} = 0$), the stresses produced on the element are given by

$$\sigma_{\mathrm{rc}} = C\,\varepsilon_{\mathrm{rc}} = C B_{\mathrm{rc}}\, q_{\mathrm{rc}}. \tag{6}$$

These stresses which are transferred to tractions along the element's boundaries may be lumped into concentrated nodal forces according to the principle of virtual work. The lumped tractions from all sides of an element can be added in a single nodal force vector T_{rc} expressed in cartesian coordinates. T_{rc} is given by

$$T_{\mathrm{rc}} = LCB_{\mathrm{rc}}\, q_{\mathrm{rc}} = P_{\mathrm{rc}}\, q_{\mathrm{rc}}, \tag{7}$$

where L is a matrix that represents the lumping of tractions to the nodes. Since Eq. (7) is valid for an arbitrary constant strain state the following equation holds

$$P_{\mathrm{rc}} = LCB_{\mathrm{rc}}. \tag{8}$$

In a constant strain state the tractions that arise along the common boundary of two neighbouring elements are equal and opposite. Hence, if the same lumping technique is used for these boundary tractions, the corresponding nodal forces should be equal and opposite as well. This ensures the pairwise cancellation

of inter-element connecting forces for joining elements during an arbitrary constant strain field as required by the patch test.

In finite element analysis, the calculation of the internal forces of an element can be done alternatively by means of its stiffness matrix k rather than surface integrals. For a rigid body constant strain state, the cartesian internal forces S_{rc} of an element are given by

$$S_{\mathrm{rc}} = kv = kG_{\mathrm{rc}}\, q_{\mathrm{rc}}. \tag{9}$$

As mentioned above, Eq. (7) guarantees inter-element force cancellation which is the basis for convergence. Consequently, to assure convergence, the element's stiffness matrix should be capable of reproducing exactly the same nodal forces given by Eq. (7), thus

$$S_{\mathrm{rc}} = T_{\mathrm{rc}}. \tag{10}$$

Since Eq. (10) should be valid for any constant strain state q_{rc}, the following equation emerges

$$kG_{\mathrm{rc}} = P_{\mathrm{rc}}. \tag{11}$$

Eq. (11) constitutes the mathematical expression of the individual element test. It is clear that the convergence requirements described in the patch test, have now been transformed into a set of linear constraints directly applicable to the stiffness matrix of a single element. Thus, the reliability of an element can now be tested without having to perform cumbersome calculations for patches of elements but rather by subjecting the element stiffness matrix through the individual element test as expressed in Eq. (11).

2.2. The non-consistent formulation

Bergan and Nygard [7] presented a simple and efficient way of deriving stiffness matrices under the light of the individual element test. The derivation makes use of the principle of minimum potential energy imposed in non-conforming shape functions that have to satisfy some orthogonality requirements, namely force and energy orthogonality. The energy orthogonality requirement can be further relaxed to lead to a non-consistent formulation, in the sense that it is not consistent with the potential energy formulation. The main steps of these formulations will be outlined here, while more details can be found in Ref. [7].

2.2.1. The conventional stiffness matrix derivation

The basis for both previously mentioned formulations is an expansion of the displacement field of the form given in Eq. (1). It should be noted that the shape functions of Eq. (1) need not satisfy inter-element compatibility but they should be linearly independent. In that case, G of Eq. (5) can be inverted and q can be written with respect to v as

$$q = Hv \Longleftrightarrow \begin{bmatrix} q_{\mathrm{rc}} \\ q_{\mathrm{h}} \end{bmatrix} = \begin{bmatrix} H_{\mathrm{rc}} \\ {\scriptstyle (n_{\mathrm{rc}} \times n_{\mathrm{t}})} \\ H_{\mathrm{h}} \\ {\scriptstyle (n_{\mathrm{h}} \times n_{\mathrm{t}})} \end{bmatrix} v. \tag{12}$$

Since $GH = HG = I$, the following expressions hold

$$H_{\mathrm{rc}} G_{\mathrm{rc}} = I_{(n_{\mathrm{rc}} \times n_{\mathrm{rc}})}, \tag{13a}$$

$$H_{\mathrm{rc}} G_{\mathrm{h}} = O_{(n_{\mathrm{rc}} \times n_{\mathrm{h}})}, \tag{13b}$$

$$H_{\mathrm{h}} G_{\mathrm{rc}} = O_{(n_{\mathrm{h}} \times n_{\mathrm{rc}})}, \tag{13c}$$

$$H_{\mathrm{h}} G_{\mathrm{h}} = I_{(n_{\mathrm{h}} \times n_{\mathrm{h}})}, \tag{13d}$$

$$G_{\mathrm{rc}} H_{\mathrm{rc}} + G_{\mathrm{h}} H_{\mathrm{h}} = I_{(n_{\mathrm{t}} \times n_{\mathrm{t}})}. \tag{13e}$$

Following the standard procedure for deriving the element stiffness matrix, the strain energy U can be written as

$$U = \frac{1}{2}\int_V \varepsilon^{\mathrm{T}} C\,\varepsilon \mathrm{d}V, \tag{14}$$

which can be expressed in terms of the generalized displacements using Eq. (3)

$$U = \frac{1}{2} q^{\mathrm{T}} \left[\int_V B_q^{\mathrm{T}}\, C\, B_q \,\mathrm{d}V \right] q = \frac{1}{2} q^{\mathrm{T}} k_q\, q, \tag{15}$$

k_q is called the generalized matrix and may be partitioned to rc- and h-modes as follows:

$$\underset{(n_{\mathrm{t}}\times n_{\mathrm{t}})}{k_q} = \begin{bmatrix} \underset{(n_{\mathrm{rc}}\times n_{\mathrm{rc}})}{k_{q\mathrm{rc}}} & \underset{(n_{\mathrm{rc}}\times n_{\mathrm{h}})}{k_{q\mathrm{rch}}} \\ \underset{(n_{\mathrm{h}}\times n_{\mathrm{rc}})}{k_{q\mathrm{rch}}^{\mathrm{T}}} & \underset{(n_{\mathrm{h}}\times n_{\mathrm{h}})}{k_{q\mathrm{h}}} \end{bmatrix}, \tag{16}$$

where

$$k_{q\mathrm{rc}} = \int_V B_{\mathrm{rc}}^{\mathrm{T}}\, C B_{\mathrm{rc}}\,\mathrm{d}V, \tag{17a}$$

$$k_{q\mathrm{rch}} = \int_V B_{\mathrm{rc}}^{\mathrm{T}}\, C B_{\mathrm{h}}\,\mathrm{d}V, \tag{17b}$$

$$k_{q\mathrm{h}} = \int_V B_{\mathrm{h}}^{\mathrm{T}}\, C B_{\mathrm{h}}\,\mathrm{d}V. \tag{17c}$$

Since the expression for the strain energy U is the same regardless the reference system used, the following equation holds

$$U = \frac{1}{2}\, q^{\mathrm{T}} k_q\, q = \frac{1}{2}\, v^{\mathrm{T}} k\, v, \tag{18}$$

where k is the cartesian stiffness matrix of the element. Knowing the relationship between the generalized modes q and the nodal degrees of freedom v, given in Eq. (12), the following transformation takes place:

$$k = H^{\mathrm{T}} k_q H = H_{\mathrm{rc}}^{\mathrm{T}} k_{q\mathrm{rc}} H_{\mathrm{rc}} + H_{\mathrm{rc}}^{\mathrm{T}} k_{q\mathrm{rch}} H_{\mathrm{h}} + H_{\mathrm{h}}^{\mathrm{T}} k_{q\mathrm{rch}}^{\mathrm{T}} H_{\mathrm{rc}} + H_{\mathrm{h}}^{\mathrm{T}} k_{q\mathrm{h}} H_{\mathrm{h}}. \tag{19}$$

Before subjecting the element stiffness matrix k through the individual element test, a relationship between $k_{q\mathrm{rc}}$ and P_{rc} is established. The expression of the potential energy for a constant strain field $\varepsilon_{\mathrm{rc}}$ takes the form

$$\Pi_{\mathrm{rc}} = \frac{1}{2}\int_V \varepsilon_{\mathrm{rc}}^{\mathrm{T}}\, C\, \varepsilon_{\mathrm{rc}}\,\mathrm{d}V - v^{\mathrm{T}} T_{\mathrm{rc}}, \tag{20}$$

where T_{rc} are the internal nodal forces expressed in Eq. (7). Using Eqs. (3) and (5) and keeping in mind that $q_{\mathrm{h}} = 0$, the expression for Π_{rc} becomes

$$\Pi_{\mathrm{rc}} = \frac{1}{2} q_{\mathrm{rc}}^{\mathrm{T}} \left[\int_V B_{\mathrm{rc}}^{\mathrm{T}}\, C\, B_{\mathrm{rc}}\,\mathrm{d}V \right] q_{\mathrm{rc}} - q_{\mathrm{rc}}^{\mathrm{T}}\, G_{\mathrm{rc}}^{\mathrm{T}} T_{\mathrm{rc}} \tag{21}$$

which gives the expression

$$\delta\Pi_{\mathrm{rc}} = 0 \Rightarrow \delta q_{\mathrm{rc}}^{\mathrm{T}} \left[\int_V B_{\mathrm{rc}}^{\mathrm{T}}\, C\, B_{\mathrm{rc}}\,\mathrm{d}V \right] q_{\mathrm{rc}} = \delta q_{\mathrm{rc}}^{\mathrm{T}}\, G_{\mathrm{rc}}^{\mathrm{T}} T_{\mathrm{rc}}. \tag{22}$$

The expression under the integral is the rigid body-constant strain stiffness matrix $k_{q\mathrm{rc}}$, as seen from Eq. (17a). Thus, Eq. (22) becomes

$$k_{q\mathrm{rc}}\, q_{\mathrm{rc}} = G_{\mathrm{rc}}^{\mathrm{T}} T_{\mathrm{rc}}. \tag{23}$$

Substituting T_{rc} from Eq. (7), the following relation is achieved

$$k_{q\mathrm{rc}} = G_{\mathrm{rc}}^{\mathrm{T}} P_{\mathrm{rc}}. \tag{24}$$

Multiplying now the element stiffness matrix k by G_{rc} and using Eqs. (13a)–(13e) and (24), one gets

$$k\,G_{\mathrm{rc}} = P_{\mathrm{rc}} + H_{\mathrm{h}}^{\mathrm{T}}\left(k_{q\mathrm{rch}}^{\mathrm{T}} - G_{\mathrm{h}}^{\mathrm{T}} P_{\mathrm{rc}}\right). \tag{25}$$

In order for the element stiffness matrix to satisfy the individual element test expressed in Eq. (11), the quantity in the parenthesis should vanish. A simple way to achieve this is to demand that the two expressions in the parenthesis vanish separately:

$$k_{q\mathrm{rch}}^{\mathrm{T}} = 0, \tag{26a}$$

$$G_{\mathrm{h}}^{\mathrm{T}} P_{\mathrm{rc}} = 0. \tag{26b}$$

The first expression is defined as the energy orthogonality condition and implies that there is no coupling between the rc-and h-modes. Keeping in mind that B_{rc} refers to the fundamental rc-modes that describe a constant state of strain and therefore is constant over the volume of the element, the energy orthogonality condition of Eq. (26a), in connection with Eq. (17b), is equivalent to the following expression

$$\int_V B_{\mathrm{h}}\,\mathrm{d}V = 0. \tag{27}$$

Eq. (26b) expresses the second orthogonality requirement which is defined as the force orthogonality condition. The physical interpretation of this requirement is that the higher order modes should be orthogonal to the forces developed under a constant strain state. Substituting Eq. (8) into Eq. (26b) and keeping in mind that matrix C is invertable, one can deduce that the force orthogonality condition of Eq. (26b) is equivalent to the following expression

$$G_{\mathrm{h}}^{\mathrm{T}} L = 0. \tag{28}$$

It should be noted that even though the derivation of the stiffness matrix mentioned above is a straightforward process emerging from the principle of minimum potential energy, no requirements of conformity have been imposed on the selection of the shape functions used.

2.2.2. The non-consistent stiffness matrix derivation

A further step when choosing the shape functions is to relax some of the constraints set by the individual element test. Let the stiffness matrix k take the form

$$k = P_{\mathrm{rc}} H_{\mathrm{rc}} + H_{\mathrm{h}}^{\mathrm{T}} k_{qh} H_{\mathrm{h}} \tag{29}$$

which implies that $k_{q\mathrm{rch}}$ is omitted without satisfying Eq. (26a). The reason for choosing this expression becomes clear when subjecting k through the individual element test. It is proved that it always satisfies the test and therefore guarantees convergence to the correct solution. A more thorough examination of k, however, gives rise to doubts concerning its symmetry. Indeed, the transformed stiffness matrix k_q that is related to the generalized modes is found to be non-symmetric

$$\underset{(n_{\mathrm{t}}\times n_{\mathrm{t}})}{k_q} = G^{\mathrm{T}} k G = \begin{bmatrix} \underset{(n_{\mathrm{rc}}\times n_{\mathrm{rc}})}{k_{q\mathrm{rc}}} & \underset{(n_{\mathrm{rc}}\times n_{\mathrm{h}})}{0} \\ \underset{(n_{\mathrm{h}}\times n_{\mathrm{rc}})}{G_{\mathrm{h}}^{\mathrm{T}} P_{\mathrm{rc}}} & \underset{(n_{\mathrm{h}}\times n_{\mathrm{h}})}{k_{qh}} \end{bmatrix} \tag{30}$$

which cannot usually be recommended for general use. Besides, the lack of symmetry in a stiffness matrix is undesirable for other reasons as well such as computational efficiency.

The generalized matrix k_q – and therefore k – becomes symmetric if the quantity $G_{\mathrm{h}}^{\mathrm{T}} P_{\mathrm{rc}}$ vanishes, or else if the force orthogonality condition of Eq. (26b) is satisfied. The generalized matrices $k_{q\mathrm{rc}}$ and $k_{q\mathrm{h}}$, that correspond to the rc- and h-modes, are the same as in Eq. (16) and they are also calculated through Eqs. (17a) and (17c), respectively. The only difference with matrix k_q given in Eq. (16) is that the coupling

term k_{qrch} vanishes without imposing the energy orthogonality condition to the selected h-modes. The present formulation is denoted in Ref. [7] as non-consistent in the sense that it does not emerge from the principle of minimum potential energy. A variety of elements presented in Ref. [7], that fall into this category, give reliable results. As will be shown in subsequent sections, the TRIC shell element can also be classified as a ''non-consistent'' element that guarantees convergence by satisfying the individual element test.

3. The TRIC element

3.1. Natural kinematics of a shell element

The key-point for the formulation of the TRIC shell element is the adoption of the so-called natural coordinate system which has the three axes parallel to the sides of the triangle as shown in Fig. 1. Apart from the natural system there are also the local elemental coordinate system, placed at the triangle's centroid, and the global cartesian coordinate system where global equilibrium refers to. Finally, for each ply of the triangle, a material coordinate system 1, 2, 3 is defined with axis 1 being parallel to the direction of the fibres. All four coordinate systems are depicted in Fig. 1. The use of these different coordinate systems makes TRIC a suitable element in modelling a multilayer anisotropic shell structure that can degenerate, as a special case, to a sandwich or a single-layer configuration.

In the natural mode method the cartesian strains have been replaced by the total natural strains. Depicted in Fig. 2 are the three total natural axial strains

$$\gamma_t = \begin{bmatrix} \gamma_{t\alpha} \\ \gamma_{t\beta} \\ \gamma_{t\gamma} \end{bmatrix}. \tag{31}$$

These strains are measured directly parallel to the triangle's sides, while by definition straining of one side leaves all other triangular sides unstrained. The total natural axial strains γ_t relate to the three in-plane cartesian strains γ according to the expression

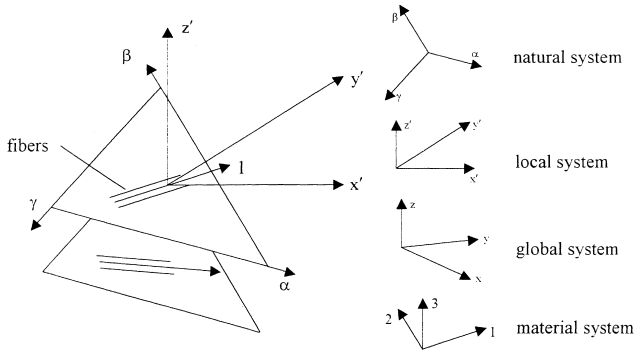

Fig. 1. The multilayer triangular TRIC element; coordinate systems.

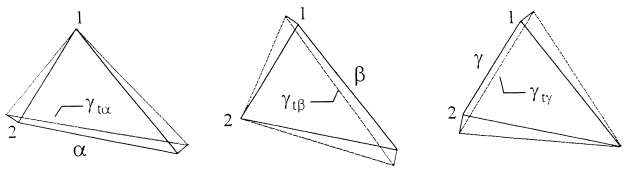

Fig. 2. Total natural axial strains.

$$\gamma_t = B\gamma \Longleftrightarrow \begin{bmatrix} \gamma_{t\alpha} \\ \gamma_{t\beta} \\ \gamma_{t\gamma} \end{bmatrix} = \begin{bmatrix} c^2_{\alpha x'} & s^2_{\alpha x'} & 2c_{\alpha x'}s_{\alpha x'} \\ c^2_{\beta x'} & s^2_{\beta x'} & 2c_{\beta x'}s_{\beta x'} \\ c^2_{\gamma x'} & s^2_{\gamma x'} & 2c_{\gamma x'}s_{\gamma x'} \end{bmatrix} \begin{bmatrix} \gamma_{xx} \\ \gamma_{yy} \\ \gamma_{xy} \end{bmatrix}, \tag{32}$$

where

$$\begin{aligned} c_{ix'} &= \cos\langle i, x'\rangle, \quad i = \alpha, \beta, \gamma, \\ s_{ix'} &= \sin\langle i, x'\rangle, \quad i = \alpha, \beta, \gamma, \end{aligned} \tag{33}$$

and $\langle \alpha, x'\rangle$, $\langle \beta, x'\rangle$, $\langle \gamma, x'\rangle$ are the angles that the triangle's edges α, β and γ form with the local x' axis, respectively.

Similarly, the total natural transverse shear strains are defined for each one of the triangle's edges

$$\gamma_s = \begin{bmatrix} \gamma_\alpha \\ \gamma_\beta \\ \gamma_\gamma \end{bmatrix}. \tag{34}$$

Fig. 3 depicts the total natural transverse shear strain for side α of the triangle. As shown, transverse shearing of one side leaves all other side angles orthogonal. The total transverse shear strains γ_s are related to the two out-of-plane transverse shear strains γ'_s via

$$\gamma_s = T_s\gamma'_s \Longleftrightarrow \begin{bmatrix} \gamma_\alpha \\ \gamma_\beta \\ \gamma_\gamma \end{bmatrix} = \begin{bmatrix} c_{\alpha x'} & s_{\alpha x'} \\ c_{\beta x'} & s_{\beta x'} \\ c_{\gamma x'} & s_{\gamma x'} \end{bmatrix} \begin{bmatrix} \gamma_{xz} \\ \gamma_{yz} \end{bmatrix}. \tag{35}$$

To the total natural axial strains γ_t correspond component natural stresses σ_c grouped in the vector

$$\sigma_c = \begin{bmatrix} \sigma_{c\alpha} \\ \sigma_{c\beta} \\ \sigma_{c\gamma} \end{bmatrix} \tag{36}$$

while the corresponding natural transverse shear stresses are

$$\sigma_s = \begin{bmatrix} \sigma_{s\alpha} \\ \sigma_{s\beta} \\ \sigma_{s\gamma} \end{bmatrix}. \tag{37}$$

The constitutive relations between the component stresses and the total strains are established by initiating the following sequence of coordinate system transformations

Material system → Local system → Natural system.

With simple geometric transformations and by contemplating the invariance of the strain energy density in the different coordinate systems, one can easily get an expression for the constitutive matrix in the natural coordinate system for both axial and transverse deformations.

$$\begin{bmatrix} \sigma_c \\ \sigma_s \end{bmatrix} = \begin{bmatrix} k_{ct} & 0 \\ 0 & X_s \end{bmatrix} \begin{bmatrix} \gamma_t \\ \gamma_s \end{bmatrix}. \tag{38}$$

Additional information for the derivation of the natural constitutive matrix can be found in Ref. [1].

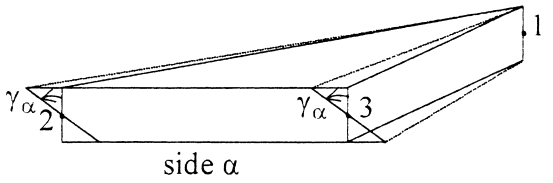

Fig. 3. Total natural transverse shear strain for side α.

3.2. Natural modes

In principle, the natural stiffness of an element is only based on deformation and not on associated rigid body motions. Thus, to the triangular shell element TRIC correspond $6\times3=18$ nodal displacements but only $18-6=12$ independent straining modes can be defined in order to satisfy all kinematic compatibility conditions. The stiffness matrix k_N corresponding to these deformations is of dimensions 12×12 and is denoted as the natural stiffness matrix. A simple congruent transformation leads to the full 18×18 cartesian stiffness matrix of the element.

In order to generate these pure deformational modes, which are called natural modes, a projection of the nodal displacements and rotations as well as the corresponding forces and moments on the triangular edges takes place. This projection on side α of the triangle is shown in Fig. 4. In a similar manner, a projection is carried out to the other two triangular sides as well. A decomposition of the rotations and moments into symmetric and antisymmetric components is then initiated, as seen in Fig. 4. From this process, the axial as well as the symmetric and antisymmetric modes of deformation are generated. Note that the antisymmetric modes comprise the antisymmetric bending and transverse shear deformations, a key-point for the shear-locking elimination as will be shown later.

The 6 rigid-body and 12 straining natural modes of the TRIC element, depicted in Figs. 5 and 6, respectively, can be grouped in the vector

$$\underset{(18\times1)}{\rho} = \begin{bmatrix} \underset{(6\times1)}{\rho_0} \\ \underset{(12\times1)}{\rho_N} \end{bmatrix}, \tag{39}$$

where ρ_0 and ρ_N represent the rigid-body and straining modes, respectively, with the following entries:

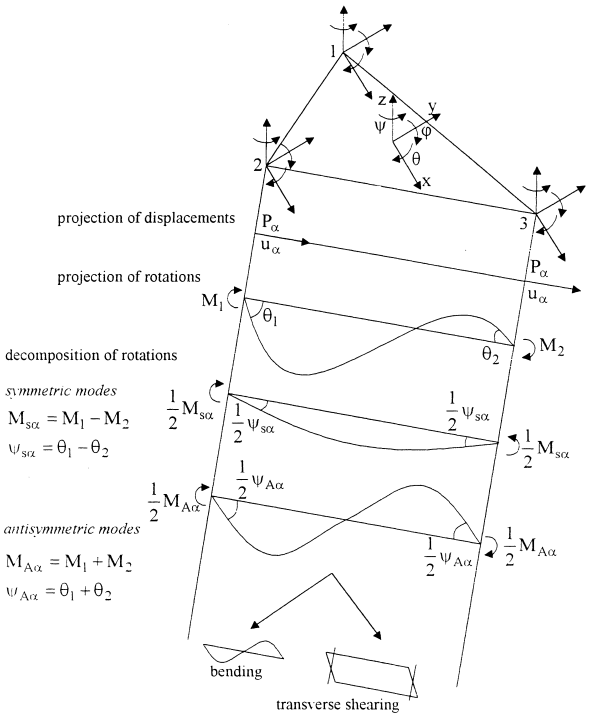

Fig. 4. Projection and decomposition of rotations and moments on triangular side α.

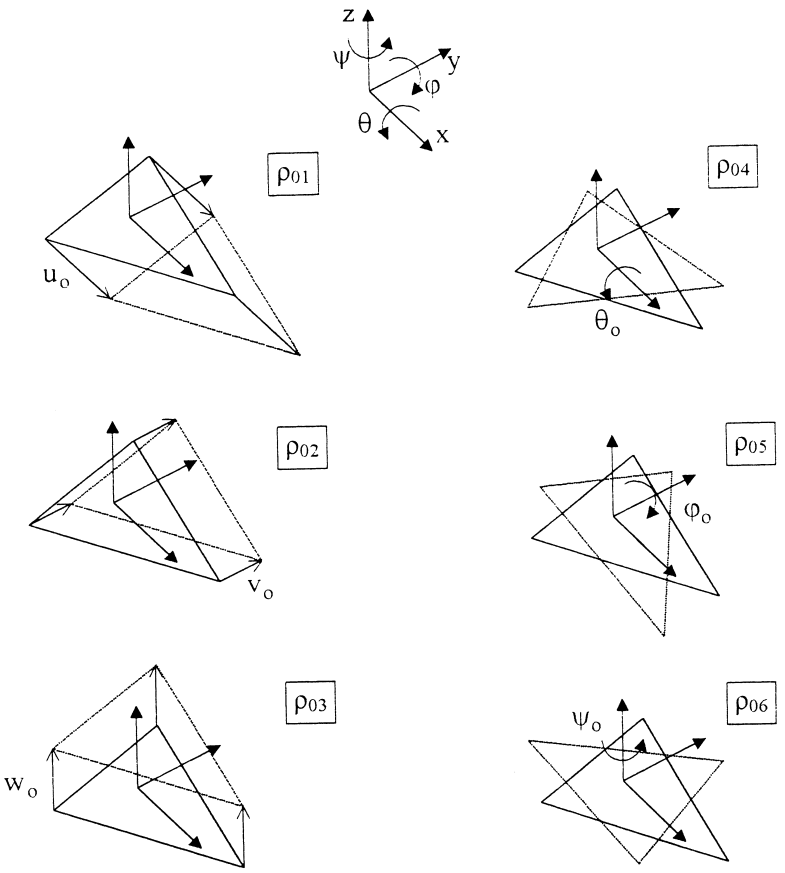

Fig. 5. The 6 natural rigid-body modes ρ_0.

$$\underset{(6\times1)}{\rho_0} = \begin{bmatrix} \rho_{01} \\ \rho_{02} \\ \rho_{03} \\ \rho_{04} \\ \rho_{05} \\ \rho_{06} \end{bmatrix} \begin{matrix} \rightarrow \text{rigid body translation along } x' \text{ axis} \\ \rightarrow \text{rigid body translation along } y' \text{axis} \\ \rightarrow \text{rigid body translation along } z' \text{ axis} \\ \rightarrow \text{rigid body rotation about } x' \text{ axis} \\ \rightarrow \text{rigid body rotation about } y' \text{ axis} \\ \rightarrow \text{rigid body rotation about } z' \text{ axis} \end{matrix} \tag{40}$$

$$\underset{(12\times1)}{\rho_N} = \begin{bmatrix} \gamma^0_{t\alpha} \\ \gamma^0_{t\beta} \\ \gamma^0_{t\gamma} \\ \psi_{s\alpha} \\ \psi_{s\beta} \\ \psi_{s\gamma} \\ \psi_{A\alpha} \\ \psi_{A\beta} \\ \psi_{A\gamma} \\ \psi_{\alpha} \\ \psi_{\beta} \\ \psi_{\gamma} \end{bmatrix} \begin{matrix} \rightarrow \text{axial straining mode along side } \alpha \\ \rightarrow \text{axial straining mode along side } \beta \\ \rightarrow \text{axial straining mode along side } \gamma \\ \rightarrow \text{sym. bending mode along side } \alpha \\ \rightarrow \text{sym. bending mode along side } \beta \\ \rightarrow \text{sym. bending mode along side } \gamma \\ \rightarrow \text{antisym. bending + shear mode along side } \alpha \\ \rightarrow \text{antisym. bending + shear mode along side } \beta \\ \rightarrow \text{antisym. bending + shear mode along side } \gamma \\ \rightarrow \text{azimuth rotational mode at node 1} \\ \rightarrow \text{azimuth rotational mode at node 2} \\ \rightarrow \text{azimuth rotational mode at node 3} \end{matrix} \tag{41}$$

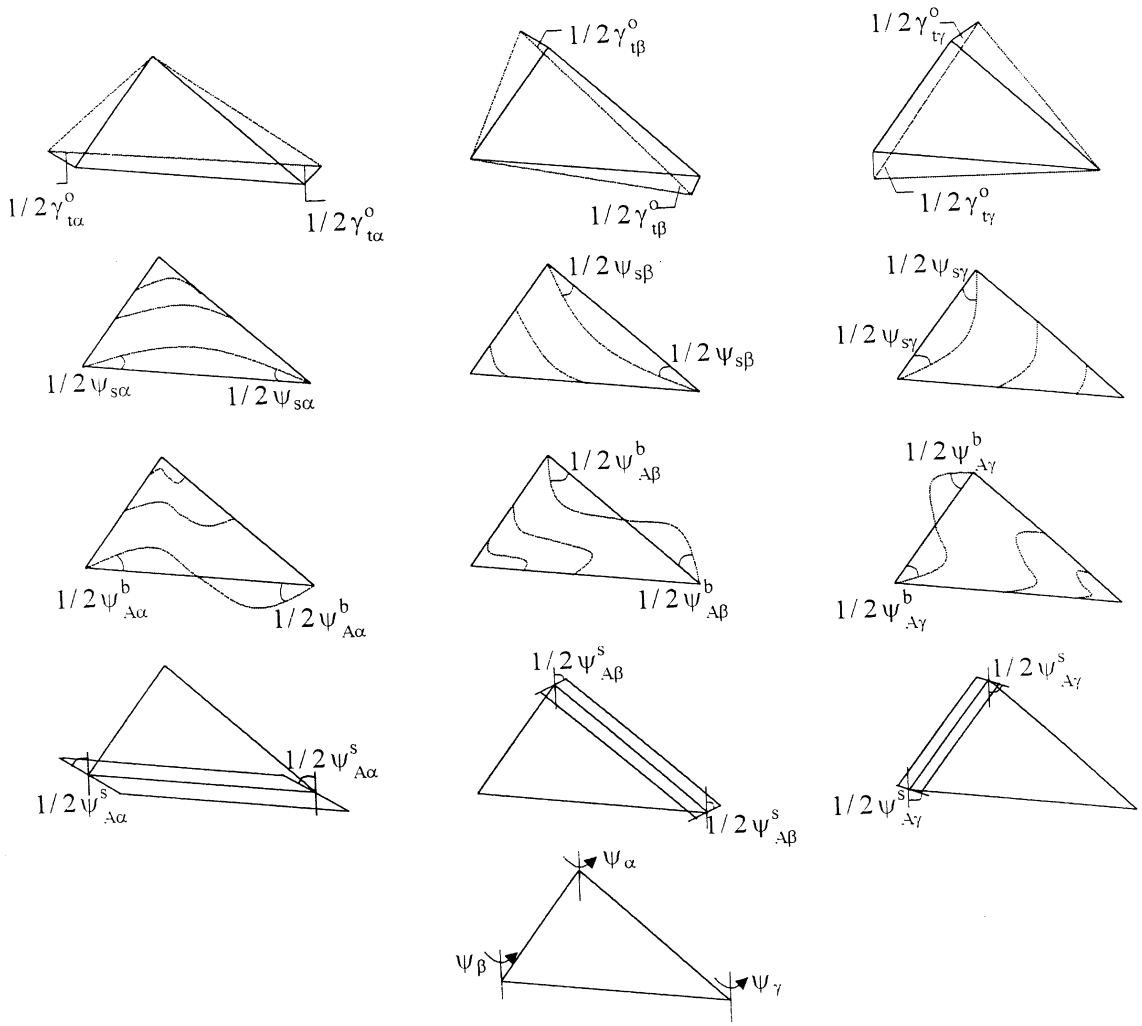

Fig. 6. The 12 natural straining modes ρ_N.

3.3. TRIC and non-consistent formulation

TRIC, as a shell element, can be regarded as a combination of a membrane and a plate element that is subjected to extension and flexure, respectively. Its membrane behaviour is represented by six translational nodal degrees of freedom in the plane of the triangle, while its flexural behaviour is described by nine degrees of freedom, one out-of-plane translation and two rotations for each node. The remaining three degrees of freedom, one for each node, are the drilling degrees of freedom that are implemented solely for computational reasons and they are treated separately from the other modes with no coupling terms between them.

From a different point of view the natural modes in Eq. (39) can be regarded as generalized displacements according to the definition given in Section 2. In that case, the 15 modes, apart from the 3 drilling degrees of freedom which will be treated in a different manner, can be separated into rigid body-constant strain modes q_{rc} and higher order modes q_h. The vector for the rigid body-constant strain modes for the TRIC element can be written as:

$$\underset{(12\times1)}{q_{\mathrm{rc}}} = \begin{bmatrix} \underset{(3\times1)}{q_{\mathrm{rm}}} \\ \underset{(3\times1)}{q_{\mathrm{rf}}} \\ \underset{(3\times1)}{q_{\mathrm{cm}}} \\ \underset{(3\times1)}{q_{\mathrm{cf}}} \end{bmatrix}, \tag{42}$$

where q_{rm} and q_{rf} group the rigid body modes associated with the membrane and the flexural behaviour of the element, respectively

$$q_{\mathrm{rm}} = \begin{bmatrix} \rho_{01} \\ \rho_{02} \\ \rho_{06} \end{bmatrix}, \tag{43}$$

$$q_{\mathrm{rf}} = \begin{bmatrix} \rho_{03} \\ \rho_{04} \\ \rho_{05} \end{bmatrix}, \tag{44}$$

while q_{cm} represents the constant strain modes for the membrane behaviour and groups the axial straining modes along the triangle's sides

$$q_{\mathrm{cm}} = \begin{bmatrix} \gamma^0_{\mathrm{t}\alpha} \\ \gamma^0_{\mathrm{t}\beta} \\ \gamma^0_{\mathrm{t}\gamma} \end{bmatrix} \tag{45}$$

and q_{cf} represents the constant strain modes for the flexural behaviour of the element, in this case the three constant-curvature modes along the triangle's sides

$$q_{\mathrm{cf}} = \begin{bmatrix} \psi_{\mathrm{s}\alpha} \\ \psi_{\mathrm{s}\beta} \\ \psi_{\mathrm{s}\gamma} \end{bmatrix}. \tag{46}$$

The adopted six membrane modes of the element are defined by the three rigid body modes q_{rm} and the three constant strain modes q_{cm}. Thus, there is no need for higher order modes for the membrane behaviour. On the other hand, the nine flexural modes of the element require, apart from the three rigid body modes q_{rf} and the three constant strain modes q_{cf}, the use of three additional higher order modes. In this case, the higher order modes correspond to the three antisymmetric bending and shearing modes along the triangle's sides

$$q_{\mathrm{h}} = \begin{bmatrix} \psi_{\mathrm{A}\alpha} \\ \psi_{\mathrm{A}\beta} \\ \psi_{\mathrm{A}\gamma} \end{bmatrix}. \tag{47}$$

The vertical displacement w, expressed in area coordinates ζ_α, ζ_β and ζ_γ shown in Fig. 7, can be written as:

$$\begin{aligned} w = {} & \frac{1}{2} l_\alpha \zeta_\beta \zeta_\gamma \psi_{\mathrm{s}\alpha} + \frac{1}{2} l_\beta \zeta_\alpha \zeta_\gamma \psi_{\mathrm{s}\beta} + \frac{1}{2} l_\gamma \zeta_\alpha \zeta_\beta \psi_{\mathrm{s}\gamma} + \frac{1}{2} l_\alpha \zeta_\beta \zeta_\gamma (\zeta_\beta - \zeta_\gamma) \psi_{\mathrm{A}\alpha} + \frac{1}{2} l_\beta \zeta_\alpha \zeta_\gamma (\zeta_\gamma - \zeta_\alpha) \psi_{\mathrm{A}\beta} \\ & + \frac{1}{2} l_\gamma \zeta_\alpha \zeta_\beta (\zeta_\alpha - \zeta_\beta) \psi_{\mathrm{A}\gamma}, \end{aligned} \tag{48}$$

where l_α, l_β and l_γ are the lengths of the sides of the triangle. According to the notation introduced by Eq. (1), the vertical displacement can be written as:

$$w = N_{\mathrm{c}} q_{\mathrm{c}} + N_{\mathrm{h}} q_{\mathrm{h}}, \tag{49}$$

where N_{c} and N_{h} are the constant strain and higher order shape functions, respectively:

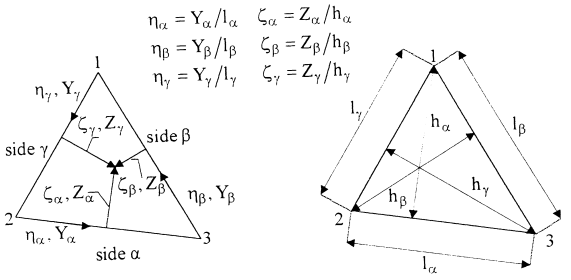

Fig. 7. Definition of the area coordinates of a triangle.

$$N_c = \left[0\ 0\ 0\ \frac{1}{2} l_\alpha \zeta_\beta \zeta_\gamma\ \frac{1}{2} l_\beta \zeta_\alpha \zeta_\gamma\ \frac{1}{2} l_\gamma \zeta_\alpha \zeta_\beta\right], \tag{50}$$

$$N_h = \frac{1}{2}\left[\, l_\alpha \zeta_\beta \zeta_\gamma (\zeta_\beta - \zeta_\gamma) \quad l_\beta \zeta_\alpha \zeta_\gamma (\zeta_\gamma - \zeta_\alpha) \quad l_\gamma \zeta_\alpha \zeta_\beta (\zeta_\alpha - \zeta_\beta) \,\right] \tag{51}$$

and q_c is the vector that groups all the constant-strain modes

$$q_c = \begin{bmatrix} q_{cm} \\ q_{cf} \end{bmatrix}. \tag{52}$$

It should be noted that the rigid body modes are not present in Eq. (49) since they give zero entries in the stiffness matrix of an element. The selection of the above shape functions for the constant strain and the higher order modes is favourable for many reasons. Firstly, they refer to directions intrinsically related to the triangle's geometry such as the three sides, ensuring in this way the objectivity of the element with respect to the selected coordinate system. Moreover, they lead to an analytical expression of matrix H of Eq. (12), which reduces significantly the computational effort for the stiffness formulation. In addition, the selected set of higher order shape functions is force orthogonal to the constant strain functions, as will be seen later.

Under a constant strain $\gamma^0_{t\alpha}$ along the triangular side α, the expression for the displacement of the middle plane of the element along the natural direction α is given by

$$u^0_\alpha = l_\alpha \left(\eta_\alpha - \frac{1}{2}\right)\gamma^0_{t\alpha}. \tag{53}$$

Similarly, for the other two natural directions the following expressions hold

$$u^0_\beta = l_\beta \left(\eta_\beta - \frac{1}{2}\right)\gamma^0_{t\beta}, \tag{54}$$

$$u^0_\gamma = l_\gamma \left(\eta_\gamma - \frac{1}{2}\right)\gamma^0_{t\gamma}. \tag{55}$$

The displacement along a natural direction of an element under combined extension and flexure is then given by the well-known formula

$$u_i = u^0_i - z\frac{\partial w}{\partial Y_i}, \quad i = \alpha, \beta, \gamma. \tag{56}$$

and the expression for the total axial strain along a natural direction is given by

$$\gamma_{ti} = \frac{\partial u_i}{\partial Y_i}, \quad i = \alpha, \beta, \gamma. \tag{57}$$

A combination of Eq. (48), (53)–(57) leads to the following expression for the total natural axial strains

$$\gamma_t = \begin{bmatrix} B_{tc} & B_{th} \\ {\scriptstyle (3\times 6)} & {\scriptstyle (3\times 3)} \end{bmatrix} \begin{bmatrix} q_c \\ {\scriptstyle (6\times 1)} \\ q_h \\ {\scriptstyle (3\times 1)} \end{bmatrix}, \tag{58}$$

where

$$B_{tc} = \begin{bmatrix} 1 & 0 & 0 & z/l_\alpha & 0 & 0 \\ 0 & 1 & 0 & 0 & z/l_\beta & 0 \\ 0 & 0 & 1 & 0 & 0 & z/l_\gamma \end{bmatrix}, \tag{59}$$

$$B_{th} = \begin{bmatrix} \dfrac{3z(\zeta_\beta - \zeta_\gamma)}{l_\alpha} & \dfrac{-z\,l_\beta \zeta_\alpha}{l_\alpha^2} & \dfrac{z\,l_\gamma \zeta_\alpha}{l_\alpha^2} \\ \dfrac{z\,l_\alpha \zeta_\beta}{l_\beta^2} & \dfrac{3z(\zeta_\gamma - \zeta_\alpha)}{l_\beta} & \dfrac{-z\,l_\gamma \zeta_\beta}{l_\beta^2} \\ \dfrac{-z\,l_\alpha \zeta_\gamma}{l_\gamma^2} & \dfrac{z\,l_\beta \zeta_\gamma}{l_\gamma^2} & \dfrac{3z(\zeta_\alpha - \zeta_\beta)}{l_\gamma} \end{bmatrix}. \tag{60}$$

It should be noted that for the derivation of Eq. (58), the following expression for the Jacobian of the area coordinates is used

$$\frac{\partial \zeta}{\partial \eta} = \begin{bmatrix} \dfrac{\partial \zeta_\alpha}{\partial \eta_\alpha} & \dfrac{\partial \zeta_\alpha}{\partial \eta_\beta} & \dfrac{\partial \zeta_\alpha}{\partial \eta_\gamma} \\ \dfrac{\partial \zeta_\beta}{\partial \eta_\alpha} & \dfrac{\partial \zeta_\beta}{\partial \eta_\beta} & \dfrac{\partial \zeta_\beta}{\partial \eta_\gamma} \\ \dfrac{\partial \zeta_\gamma}{\partial \eta_\alpha} & \dfrac{\partial \zeta_\gamma}{\partial \eta_\beta} & \dfrac{\partial \zeta_\gamma}{\partial \eta_\gamma} \end{bmatrix} = \begin{bmatrix} 0 & 1 & -1 \\ -1 & 0 & 1 \\ 1 & -1 & 0 \end{bmatrix}. \tag{61}$$

From the expression of B_{th}, it is clear that $\int_V B_{th}\,dV \neq 0$. Therefore, TRIC does not satisfy the energy orthogonality condition of Eq. (26a). On the other hand, it can be verified that the force orthogonality condition is satisfied. This is shown in the following manner. In order for the higher order modes to be force orthogonal, Eq. (26b) or its equivalent Eq. (28) should be satisfied. The expression for matrix L, that represents the lumping of the tractions, acting along the element's boundaries, to the nodes, is the same for all triangular bending elements and is given by

$$L = \frac{1}{2}\begin{bmatrix} 0 & 0 & 0 \\ 0 & x_\alpha & -y_\alpha \\ y_\alpha & 0 & -x_\alpha \\ 0 & 0 & 0 \\ 0 & x_\beta & -y_\beta \\ y_\beta & 0 & -x_\beta \\ 0 & 0 & 0 \\ 0 & x_\gamma & -y_\gamma \\ y_\gamma & 0 & -x_\gamma \end{bmatrix}, \tag{62}$$

where

$$x_\alpha = x_3 - x_2, \quad x_\beta = x_1 - x_3, \quad x_\gamma = x_2 - x_1,$$
$$y_\alpha = y_3 - y_2, \quad y_\beta = y_1 - y_3, \quad y_\gamma = y_2 - y_1,$$

where x_1, x_2, x_3, y_1, y_2, y_3 are the x and y coordinates of the three vertices of the triangle, respectively.

The expression for G_h that relates the nodal displacements w_i, θ_i, ϕ_i $(i = 1, 2, 3)$ of the three vertices to the higher order modes is easily found using Eq. (48) and keeping in mind that for the rotations about x and y axes, the following relations hold

$$\begin{aligned} &\text{rotation about } x \text{ axis}: \quad \theta_i = \left.\frac{\partial w}{\partial y}\right|_i, \quad i = 1,2,3, \\ &\text{rotation about } y \text{ axis}: \quad \varphi_i = -\left.\frac{\partial w}{\partial x}\right|_i, \quad i = 1,2,3. \end{aligned} \tag{63}$$

Knowing the expression of the derivatives of the area coordinates with respect to the cartesian coordinates

$$\frac{\partial \zeta_i}{\partial x} = -\frac{y_i}{2\Omega}, \quad i = \alpha,\beta,\gamma, \tag{64a}$$

$$\frac{\partial \zeta_i}{\partial y} = \frac{x_i}{2\Omega}, \quad i = \alpha,\beta,\gamma, \tag{64b}$$

the expression for G_{h} is established as follows

$$G_{\mathrm{h}} = \frac{1}{4\Omega}\begin{bmatrix} 0 & 0 & 0 \\ 0 & -x_\gamma l_\beta & x_\beta l_\gamma \\ 0 & -y_\gamma l_\beta & y_\beta l_\gamma \\ 0 & 0 & 0 \\ x_\gamma l_\alpha & 0 & -x_\alpha l_\gamma \\ y_\gamma l_\alpha & 0 & -y_\alpha l_\gamma \\ 0 & 0 & 0 \\ -x_\beta l_\alpha & x_\alpha l_\beta & 0 \\ -y_\beta l_\alpha & y_\alpha l_\beta & 0 \end{bmatrix}, \tag{65}$$

where Ω is the area of the triangle. Executing the multiplication of Eq. (28) with G_{h} and L taken from Eqs. (65) and (62), respectively, the force orthogonality condition can be easily verified.

It is therefore shown that the non-conforming shape functions used for the interpolation of the displacement field for the TRIC shell element satisfy the force orthogonality condition. Thus, according to the non-consistent formulation, the stiffness matrix of TRIC always satisfies the individual element test and therefore guarantees convergence to the exact solution.

3.4. Natural stiffness matrix k_N

After the definition of the generalized displacements, one could easily proceed to the formulation of the generalized matrix of Eq. (16), which in this case is denoted as the natural stiffness matrix

$$\underset{(12\times12)}{k_{\mathrm{N}}} = \begin{bmatrix} \underset{(6\times6)}{k_{q\mathrm{c}}} & 0 & 0 \\ 0 & \underset{(3\times3)}{k_{q\mathrm{h}}} & 0 \\ 0 & 0 & \underset{(3\times3)}{k_{\mathrm{az}}} \end{bmatrix}. \tag{66}$$

The difference between k_{N} and k_q of Eq. (16) is that k_{N} is of order 12×12 instead of 18×18 ($n_{\mathrm{t}} = 18$), since the six rigid body modes that are included in k_q do not participate in the formation of k_{N} according to the natural mode method, while k_{az} that refers to the three drilling degrees of freedom is incorporated in Eq. (66).

Before dealing separately, in the following sections, with all submatrices involved in k_{N} it should be noted that although it is the stiffness matrix k in the global coordinate system that is used in the final finite element equations, the knowledge of k_{N} can also provide some valuable information. In fact, k_{N} is a sparse matrix of only 33 non-zero entries that can be stored for each element separately. Since it refers to pure deformational modes, its use can provide an insight on the deformation patterns of the structure and on ways of enhancing its performance according to the dominating straining modes.

3.4.1. Constant strain stiffness matrix $k_{q\mathrm{c}}$

The constant strain stiffness matrix $k_{q\mathrm{c}}$ refers to the constant strain modes of Eq. (52). According to Eq. (17a), $k_{q\mathrm{c}}$ is formed via

$$\underset{(6\times6)}{k_{qc}} = \int_V B_{tc}^T k_{ct} B_{tc} \mathrm{d}V, \tag{67}$$

where B_{tc} and k_{ct} are defined in Eqs. (59) and (38), respectively. Analytical expressions for all terms of k_{qc} in Eq. (67) are straightforward and can be found in Ref. [1].

3.4.2. Higher order stiffness matrix k_{qh}

The formulation introduced by Argyris deals with the transverse shear deformations in a way that eliminates the shear-locking effect. However, the derivation of k_{qh} for the TRIC element in Ref. [1] was based on more or less heuristic considerations and deviates from the standard procedure expressed in Eq. (17c). In this section, the locking-free stiffness terms of the element will be derived following the standard finite element procedure. This will be shown first for the case of a beam element, which is suitable for a more physical interpretation, and then the derivation will easily be extended to the triangular shell element.

Higher order terms for the beam element. The 2-node beam element shown in Fig. 8(a) is subjected to bending in the x–z plane. According to Timoshenko's theory, its cartesian strains are described as:

$$\gamma_{xx} = -z\frac{\partial\theta(x)}{\partial x}, \tag{68}$$

$$\gamma_{xz} = -\theta(x) + \frac{\partial w}{\partial x}, \tag{69}$$

where $\theta(x)$ denotes the rotation of the cross-section and $w(x)$ the vertical displacement of the middle plane. Under an assumed symmetric bending with two equal and opposite moments at the two ends, as depicted in Fig. 8(b), the shear force Q is equal to zero along the beam resulting in zero transverse shear stress σ_{xz} and zero transverse shear strain γ_{xz}. From Eq. (69) it is clear for this case that

$$\theta(x) = \frac{\partial w}{\partial x}. \tag{70}$$

Substituting in Eq. (68), the axial strain is then given by

$$\gamma_{xx} = -z\frac{\partial^2 w}{\partial x^2} \tag{71}$$

an expression which is identical to that of Bernoulli's theory.

In Fig. 8(c) antisymmetric flexure takes place by imposing two equal moments at the two ends of the beam. Equilibrium is satisfied with a shear force Q that is constant along the beam and is given by

$$Q = -\frac{2M_A}{l}, \tag{72}$$

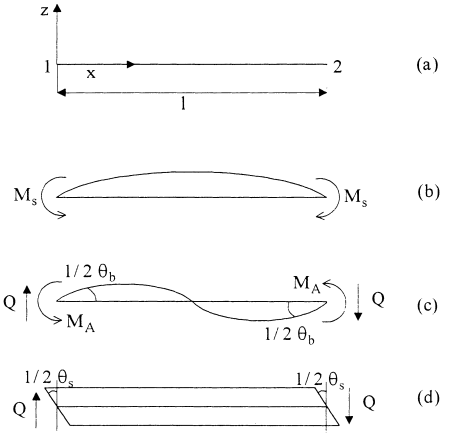

Fig. 8. Symmetric and antisymmetric bending of beam element.

where M_A is the antisymmetric moment and l is the length of the beam. Hence, both σ_{xz} and γ_{xz} are constant. According to Fig. 8(d), let

$$\gamma_{xz} = \text{constant} = -1/2\theta_s.$$

Then, the following relations hold

$$\gamma_{xz} = \frac{\sigma_{xz}}{\chi G} = \frac{Q}{\chi GA} \Rightarrow -\frac{1}{2}\theta_s = -\frac{2M_A}{\chi GAl}, \tag{73}$$

where G is the shear modulus, A the area of the cross-section and χ the shear correction factor of the beam.

From Eq. (69), it can be observed that the total rotation for each cross-section is the sum of the rotation from Bernoulli's theory, namely $\partial w/\partial x$ and of the constant shear rotation $1/2\theta_s$. Let the Bernoulli rotation in Eq. (69) be denoted as $\partial w/\partial x = 1/2\theta_b$ at the beam's edges, where θ_b is the rotation of the cross-section due to antisymmmetric bending. From Eq. (69) and Fig. 8(c) and (d), it can be deduced that

$$\frac{1}{2}\theta = \frac{1}{2}\theta_b + \frac{1}{2}\theta_s. \tag{74}$$

The rotation $1/2\theta_b$ can easily be expressed as a function of M_A

$$\frac{1}{2}\theta_b = \frac{M_A l}{6EI}, \tag{75}$$

where E is Young's modulus and I the moment of inertia of the beam's cross section.

Furthermore, Eqs. (73) and (75) can also be written as:

$$\theta_s = k_s^{-1} M_A, \tag{76}$$

$$\theta_b = k_b^{-1} M_A, \tag{77}$$

where

$$k_s = \frac{\chi GAl}{4}, \tag{78}$$

$$k_b = \frac{3EI}{l}. \tag{79}$$

Substituting Eqs. (76) and (77) into Eq. (74), one gets

$$\theta = \left(k_b^{-1} + k_s^{-1}\right) M_A \Rightarrow M_A = k_A \theta, \tag{80}$$

where k_A is denoted as the natural antisymmetric stiffness of the beam

$$k_A = \frac{1}{1/k_b + 1/k_s} = \frac{3EI}{l(1+\lambda)} \quad \text{and} \quad \lambda = \frac{12EI}{l^2 \chi GA}, \tag{81}$$

where λ is called the beam shearing coefficient. For a thin beam λ goes towards zero and the antisymmetric stiffness k_A approaches the bending antisymmetric stiffness k_b of the beam. Thus, k_A provides an expression for the natural stiffness of the antisymmetric bending and shear modes that circumvents the transverse shear-locking phenomenon.

Higher order terms for the TRIC element. Back to TRIC shell element, the symmetric and antisymmetric modes shown in Fig. 6 are similar to those shown in Fig. 8 for the beam element. By analogy, the triangular element can be regarded as if it consists of three fictitious beams along the sides of the triangle. Similarly to Eq. (74), the total antisymmetric rotations at the edges of each one of the triangle's sides, which are expressed via the three higher order modes q_h of Eq. (47), can split into two components, namely the antisymmetric bending rotations and the shear rotations. This is expressed by

$$q_{\mathrm{h}} = q_{\mathrm{h}}^{\mathrm{b}} + q_{\mathrm{h}}^{\mathrm{s}} \Rightarrow \begin{bmatrix} \psi_{\mathrm{A}\alpha} \\ \psi_{\mathrm{A}\beta} \\ \psi_{\mathrm{A}\gamma} \end{bmatrix} = \begin{bmatrix} \psi^{b}_{\mathrm{A}\alpha} \\ \psi^{b}_{\mathrm{A}\beta} \\ \psi^{b}_{\mathrm{A}\gamma} \end{bmatrix} + \begin{bmatrix} \psi^{s}_{\mathrm{A}\alpha} \\ \psi^{s}_{\mathrm{A}\beta} \\ \psi^{s}_{\mathrm{A}\gamma} \end{bmatrix}. \tag{82}$$

In turn, the antisymmetric rotations give rise to antisymmetric moments M_{A}. Then, the following relation holds

$$M_{\mathrm{A}} = k_{q\mathrm{h}}\, q_{\mathrm{h}}. \tag{83}$$

As in Eqs. (76) and (77), $q_{\mathrm{h}}^{\mathrm{b}}$ and $q_{\mathrm{h}}^{\mathrm{s}}$ can be expressed as functions of M_{A}

$$q_{\mathrm{h}}^{\mathrm{b}} = \left(k_{q\mathrm{h}}^{\mathrm{b}}\right)^{-1} M_{\mathrm{A}}, \tag{84}$$

$$q_{\mathrm{h}}^{\mathrm{s}} = \left(k_{q\mathrm{h}}^{\mathrm{s}}\right)^{-1} M_{\mathrm{A}}, \tag{85}$$

where $k_{q\mathrm{h}}^{\mathrm{b}}$ and $k_{q\mathrm{h}}^{\mathrm{s}}$ are the natural stiffness matrices associated to the antisymmetric bending modes and the shear modes, respectively.

Using the expression for the constitutive matrix in the natural coordinate system given in Eq. (38), the expression for the strain energy in the case of the TRIC element can be written as

$$U = \frac{1}{2}\int_V \varepsilon^{\mathrm{T}} C\, \varepsilon \mathrm{d}V = \frac{1}{2}\int_V \gamma_{\mathrm{t}}^{\mathrm{T}} k_{\mathrm{ct}} \gamma_{\mathrm{t}} \mathrm{d}V + \frac{1}{2}\int_V \gamma_{\mathrm{s}}^{\mathrm{T}} \chi_{\mathrm{s}} \gamma_{\mathrm{s}}\, \mathrm{d}V = U_{\mathrm{t}} + U_{\mathrm{s}}, \tag{86}$$

where U_{t} and U_{s} denote the strain energy due to the total axial strains γ_{t} and the natural transverse shear strains γ_{s}, respectively. The antisymmetric bending stiffness matrix $k_{q\mathrm{h}}^{\mathrm{b}}$ is calculated via the strain energy U_{t} and takes the form

$$k_{q\mathrm{h}}^{\mathrm{b}} = \int_V B_{\mathrm{th}}^{\mathrm{T}} k_{\mathrm{ct}} B_{\mathrm{th}}\, \mathrm{d}v, \tag{87}$$

where B_{th} is defined in Eq. (60). For the derivation of the above expression for $k_{q\mathrm{h}}^{\mathrm{b}}$, Eq. (58) is used with the exception that the antisymmetric bending modes $q_{\mathrm{h}}^{\mathrm{b}}$ take the place of the total antisymmetric modes q_{h}. This replacement is valid, since it does not affect the calculation of the axial strains γ_{t}, as can be seen in Fig. 9. According to Fig. 9, the axial strain is calculated as:

$$\varepsilon = \frac{\Delta x}{\Delta x_0} = \frac{\theta_2 z - \theta_1 z}{\Delta x_0} = \frac{(\theta_{\mathrm{b}2} + \theta_{\mathrm{s}2} - \theta_{\mathrm{b}1} - \theta_{\mathrm{s}1}) z}{\Delta x_0}. \tag{88}$$

As mentioned above, the shear strain in antisymmetric bending is constant, giving $\theta_{1\mathrm{s}} = \theta_{2\mathrm{s}}$. This results in

$$\varepsilon = \frac{(\theta_2 - \theta_1) z}{\Delta x_0} = \frac{(\theta_{\mathrm{b}2} - \theta_{\mathrm{b}1}) z}{\Delta x_0} \tag{89}$$

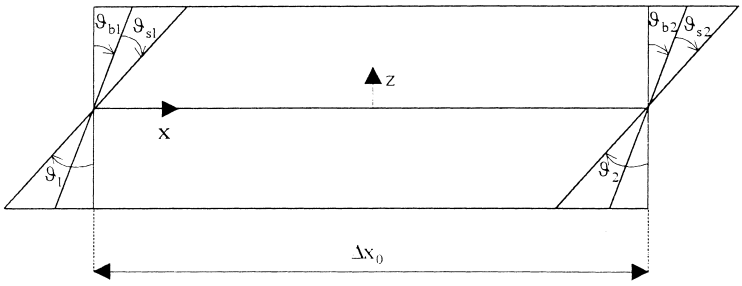

Fig. 9. Axial straining due to antisymmetric bending.

which has the consequence that the antisymmetric bending modes $q_{\mathrm{h}}^{\mathrm{b}}$ can be used in Eq. (58), instead of q_{h}, without affecting the outcome of the multiplication.

The natural transverse shear stiffness matrix $k_{q\mathrm{h}}^{\mathrm{s}}$ is calculated via the strain energy U_{s}, using the following expression that relates the natural transverse shear strains γ_{s} to the shear modes $q_{\mathrm{h}}^{\mathrm{s}}$

$$\begin{bmatrix} \gamma_\alpha \\ \gamma_\beta \\ \gamma_\gamma \end{bmatrix} = \begin{bmatrix} \frac{1}{2}\psi_{\mathrm{A}\alpha}^{\mathrm{s}} \\ \frac{1}{2}\psi_{\mathrm{A}\beta}^{\mathrm{s}} \\ \frac{1}{2}\psi_{\mathrm{A}\gamma}^{\mathrm{s}} \end{bmatrix} \Rightarrow \gamma_{\mathrm{s}} = B_{\mathrm{sh}}\, q_{\mathrm{h}}^{\mathrm{s}}, \tag{90}$$

where

$$B_{\mathrm{sh}} = \begin{bmatrix} 1/2 & 0 & 0 \\ 0 & 1/2 & 0 \\ 0 & 0 & 1/2 \end{bmatrix}, \tag{91}$$

$k_{q\mathrm{h}}^{\mathrm{s}}$ is then calculated by substituting Eq. (90) in the expression for U_{s}, as

$$k_{q\mathrm{h}}^{\mathrm{s}} = \int_V B_{\mathrm{sh}}^{\mathrm{T}}\, \mathbf{X}_{\mathrm{s}}\, B_{\mathrm{sh}}\, \mathrm{d}V. \tag{92}$$

The final analytical expressions for both $k_{q\mathrm{h}}^{\mathrm{b}}$ and $k_{q\mathrm{h}}^{\mathrm{s}}$ can be found in Ref. [1]. It should be noted that, since the transverse shear stresses at the top and bottom surfaces of a shell element vanish, the natural transverse shear stiffness matrix $k_{q\mathrm{h}}^{\mathrm{s}}$ needs to be multiplied by shear correction factors. According to the natural mode method, there are three natural shear correction factors, one for each triangular side, which are defined through the correction of the transverse shear energy with regard to the exact energy according to the beam theory. The whole procedure for the evaluation of the shear correction factors is described in detail in Ref. [1].

Having obtained k_{qh}^{b} and k_{qh}^{s}, the expression for the natural antisymmetric stiffness $k_{q\mathrm{h}}$ can be written in an analogous way to that of Eq. (81)

$$k_{q\mathrm{h}} = \left[\left[k_{q\mathrm{h}}^{\mathrm{b}} \right]^{-1} + \left[k_{q\mathrm{h}}^{\mathrm{s}} \right]^{-1} \right]^{-1}. \tag{93}$$

The inversions involved in Eq. (93) can be very easily performed analytically with marginal computing cost since the matrices are of dimensions 3×3. Furthermore, $k_{q\mathrm{h}}$ is free from the undesirable shear-locking effect for the same reasons that were mentioned in the case of the beam element.

3.4.3. Azimuth stiffness matrix k_{az}

The drilling degrees of freedom are not involved in the derivation of the element's stiffness. However, these degrees of freedom should be retained, solely for computational reasons. In the case of the TRIC element, the assignment of stiffness terms to the drilling degrees of freedom is done in a way that is consistent with the natural mode method. Three rotational springs with the same stiffness k_z are considered at the three vertices of the triangle and they are used to simulate the in-plane rotation about z axis. The corresponding natural modes consist of a unit rotation about z axis at each one of the three vertices

$$q_{\mathrm{az}} = \begin{bmatrix} \psi_\alpha \\ \psi_\beta \\ \psi_\gamma \end{bmatrix}. \tag{94}$$

The azimuth stiffness matrix k_{az} is then calculated as

$$k_{\mathrm{az}} = k_z \begin{bmatrix} 1 & -1/2 & -1/2 \\ -1/2 & 1 & -1/2 \\ -1/2 & -1/2 & 1 \end{bmatrix} \tag{95}$$

with k_z having an arbitrary but small enough value, compared to the rest of the stiffness terms, so that it will produce a negligible effect on the final equilibrium equations.

$$k_z = 10^{-6}\Omega \max\left\{ \frac{1}{l_\alpha^2}\int_{-h/2}^{h/2} z^2 k_{\alpha\alpha}\,\mathrm{d}z,\ \frac{1}{l_\beta^2}\int_{-h/2}^{h/2} z^2 k_{\beta\beta}\,\mathrm{d}z,\ \frac{1}{l_\gamma^2}\int_{-h/2}^{h/2} z^2 k_{\gamma\gamma}\,\mathrm{d}z \right\}, \tag{96}$$

where h is the thickness of the shell element and $k_{\alpha\alpha}, k_{\beta\beta}, k_{\gamma\gamma}$ are the diagonal terms of k_{ct}. It should be noted that these modes are defined exclusively for computational reasons and this is the reason why the coupling terms connecting these degrees of freedom with the rest of the modes are set equal to zero.

3.5. Cartesian stiffness matrix k

The cartesian stiffness matrix k in the local coordinate system can be found using the following transformation

$$k = H^T k_{\mathrm{N}} H, \tag{97}$$

where H is the matrix that relates the natural straining modes ρ_{N} to the cartesian nodal displacements v

$$\underset{(18\times 1)}{v} = \begin{bmatrix} u \\ v \\ w \\ \theta \\ \varphi \\ \psi \end{bmatrix}_i \qquad i = 1,2,3 \tag{98}$$

with u_i, v_i, w_i being the three nodal translations and θ_i, φ_i, ψ_i the three nodal rotations of node i. The calculation of H is done using strictly geometrical arguments and can be expressed analytically (see Ref. [1]).

A final transformation leads to the global elemental stiffness $\bar{k}$

$$\bar{k} = T_{06}^T k\, T_{06}, \tag{99}$$

where T_{06} is an 18×18 hyper diagonal matrix of the form

$$T_{06} = \begin{bmatrix} T_0 & 0 & 0 & 0 & 0 & 0 \\ 0 & T_0 & 0 & 0 & 0 & 0 \\ 0 & 0 & T_0 & 0 & 0 & 0 \\ 0 & 0 & 0 & T_0 & 0 & 0 \\ 0 & 0 & 0 & 0 & T_0 & 0 \\ 0 & 0 & 0 & 0 & 0 & T_0 \end{bmatrix} \tag{100}$$

and T_0 is the 3×3 matrix with the direction cosines formed between the local and the global cartesian coordinate system according to Fig. 1.

4. Numerical examples

In order to test the robustness, accuracy and efficiency of the TRIC element, a number of numerical tests are presented for a set of representative plate and shell problems. As mentioned before, the present element passes the patch test by virtue of its inherent properties. Nevertheless, comparisons with existing analytical solutions as well as with numerical results reported for other shell finite elements are presented, showing the fast convergence characteristics of the proposed element. Furthermore, benchmark test examples which are prone to induce locking are included in an attempt to show the locking-free characteristics of the TRIC element. Finally, a comparison of the computing time spent for the formation of the stiffness matrix between the TRIC element and the 8-node serendipity shell element demonstrates TRIC's excellent computational performance.

4.1. Clamped isotropic plate under concentrated load and uniform pressure

The vertically loaded rectangular plate under uniform pressure q and concentrated load P, shown in Fig. 10, has become a de facto standard test and has been frequently studied in the technical literature. The geometrical and material data for the clamped plate is shown in Fig. 10, while due to symmetry, only one quarter of the plate is discretized for both loading cases. The slenderness ratio used is extremely small ($h/a = 1/20\,000$) and although it is outside the range of practical significance and application of a plate theory, it is chosen to demonstrate the shear locking-free behaviour of the proposed element. The central displacement under the concentrated load and the uniform pressure as well as the computed moment at the center of the plate due to the uniform pressure are compared to the analytical solutions given by Kirchhoff:

Central displacement due to concentrated load P

$$w_c^{\text{ref}}(P) = 0.0056\frac{Pa^2}{D}.$$

Central displacement and moment due to uniformly distributed pressure q

$$w_c^{\text{ref}}(q) = 0.00126\frac{qa^4}{D},$$

$$M_x^{\text{ref}}(q) = 0.021\,qa^2,$$

where a is the length of the square plate and D is called the plate stiffness and is given by

$$D = \frac{Eh^3}{12(1-\nu^2)}.$$

Table 1 shows the aforementioned quantities normalized with respect to the exact solution for successive mesh refinements. The results obtained show good agreement even for coarse meshes.

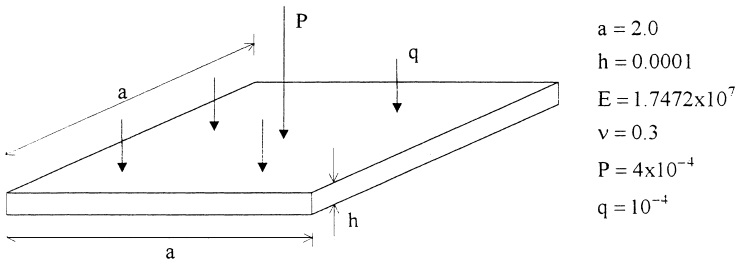

Fig. 10. Material and geometrical data of clamped isotropic plate.

Table 1
Clamped isotropic plate; central displacement under concentrated load (P) and central displacement and moment under uniform pressure (q) normalized with respect to the exact solution

Mesh[a]	d.o.f.	$w_c(P)$	$w_c(q)$	$M_x(q)$
2×2	16	1.008	1.158	0.849
4×4	80	1.005	1.046	0.975
6×6	192	1.004	1.023	0.988
8×8	352	1.003	1.015	0.992

[a] Quarter plate.

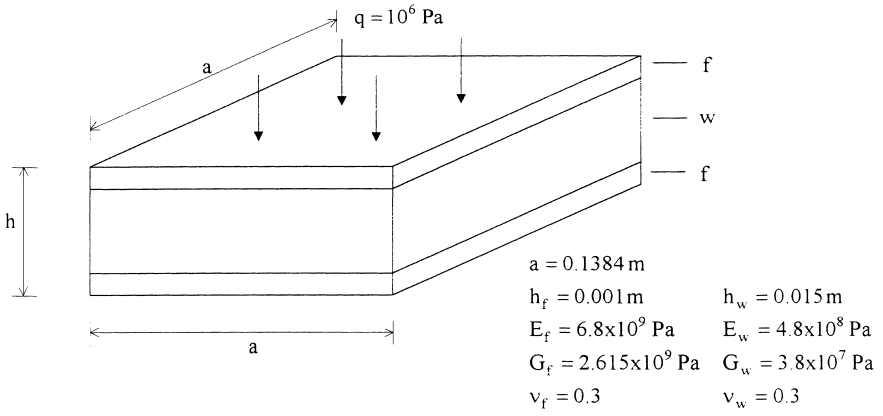

Fig. 11. Material and geometrical data of thick sandwich plate.

Table 2
Simply supported sandwich plate under uniform load; central displacement and moment normalized with respect to the exact solution

Mesh[a]	d.o.f.	$w_c(q)$	$M_x(q)$
2×2	28	0.988	0.834
4×4	104	0.992	0.994
6×6	228	0.992	1.022
8×8	400	0.992	1.026

[a] Quarter plate.

4.2. Simply supported thick sandwich plate under uniform pressure load

TRIC is subjected to a second test for a thick sandwich plate, shown in Fig. 11. The panel, which consists of two thin outer faces and a thicker core with different material properties is subjected to uniformly distributed pressure. The sandwich plate is a fairly thick panel ($h/a = 1/8.14$) and therefore represents a challenging test for simple shear deformable elements. Again, only one quarter of the plate is discretized, while the central displacement and the central moment are compared to the analytical solution ($w_c^{ref} = 31.45$, $M_x^{ref} = 3668.3$) given by Reissner taking into account transverse shear deformations. As can be seen in Table 2, good agreement and fast convergence to the reference solution is obtained. It is worthwhile noticing that due to the structure's material properties, (layers with different material characteristics) the shear correction factors that should be used deviate from the standard value of 5/6 that holds for isotropic behaviour. In the present formulation the shear correction factors were found equal to 0.11.

4.3. Rectangular plate with cross-ply and antisymmetric angle-ply laminates

This numerical example was presented by Braun, Bischoff and Ramm [11] as a benchmark test for anisotropic behaviour especially when no symmetry exists across the thickness, as in the case of the antisymmetric plies. The rectangular plate is subjected to uniform pressure load ($p = 0.1$ psi), while the problem data and boundary conditions for the full plate with the cross-ply and antisymmetric laminates are given in Figs. 12(a) and (b), respectively. Three different cross-ply and two different antisymmetric laminations with different orientation of the plies are considered. Table 3(a) and (b) show the central displacement normalized with respect to the exact solution, for the case of the cross-ply and antisymmetric laminates, respectively. The reference solution is given by Reddy and Pandey [12], according to the lamination used, as follows:

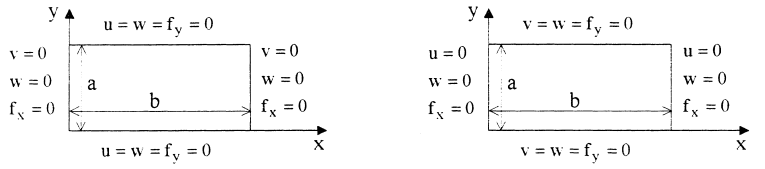

a) cross - ply laminates b) antisymmetric angle - ply laminates

$a = 5\,\text{in}$ $b = 9\,\text{in}$ ply thickness $h_L = 0.005\,\text{in}$

$E_1 = 19.2\text{x}10^6$ psi $E_2 = E_3 = 1.56\text{x}10^6$ psi

$G_{23} = 0.49\text{x}10^6$ psi $G_{12} = G_{13} = 0.82\text{x}10^6$ psi

$\nu_{23} = 0.49$ $\nu_{12} = \nu_{13} = 0.24$

Fig. 12. Material and geometrical data of rectangular plate with cross-ply and antisymmetric angle-ply laminates.

Table 3
(a) Rectangular plate with cross-ply laminates under uniform load; central displacement normalized with respect to the exact solution for three different laminations; (b) rectangular plate with antisymmetric angle-ply laminates under uniform load; central displacement normalized with respect to the exact solution for two different laminations

Mesh[a]	d.o.f.	0°/90°	0°/90°/0°/90°	0°/90°/90°/0°	15°/−15°/15°/−15°	45°/−45°
2×2	29	0.889	0.940	0.908	0.940	0.908
4×4	105	0.977	0.993	0.983	0.993	0.983
6×6	229	0.991	1.000	0.996	1.000	0.996
8×8	401	0.996	1.000	1.000	1.000	1.000

[a] Quarter plate.

Lamination	Exact
0°/90°	1.884
0°/90°/0°/90°	0.134
0°/90°/90°/0°	0.229
15°/−15°/15°/−15°	0.251
45°/−45°	1.600

4.4. Simply supported thick laminated plate under sinusoidal loading

The rectangular laminated plate depicted in Fig. 13 is subjected to sinusoidally distributed pressure load $p(x,y) = p_0 \sin \pi x/a \sin \pi y/b$ where a and b are the two in-plane dimensions of the plate. The panel consists of three layers with 0°/90°/0° orientation of the plies. The same test is also presented by Braun et al. [11], where different values are used for the slenderness ratio of the plate. Here, a relatively large value ($h/a =$ 1/4) is adopted for the slenderness ratio, while the central displacement is compared to the three-dimensional elasticity solution ($w^{\text{ref}} = 3.61 \times 10^{-5}$) given by Pagano [13]. Table 4 shows the normalized central displacement for different mesh refinements.

4.5. Pinched cylinder

A cylinder supported by rigid end-diaphragms is loaded with two opposite concentrated loads. The geometrical and material properties of the cylinder are depicted in Fig. 14. The small slenderness ratio (h/R = 1/100) of the cylindrical shell is chosen to demonstrate the capability of TRIC element to overcome shear and membrane-locking phenomena. In Table 5, the displacement under the applied load, normalized

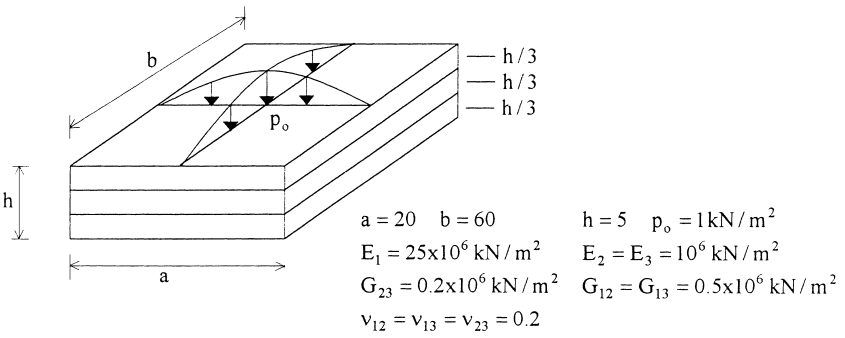

Fig. 13. Material and geometrical data of thick laminated plate under sinusoidal loading.

Table 4
Simply supported thick laminated plate under sinusoidal loading; central displacement normalized with respect to the exact solution

Mesh[a]	d.o.f.	w
2×2	28	1.285
4×4	104	1.207
6×6	228	1.121
8×8	400	1.072
10×10	620	1.044

[a] Quarter plate.

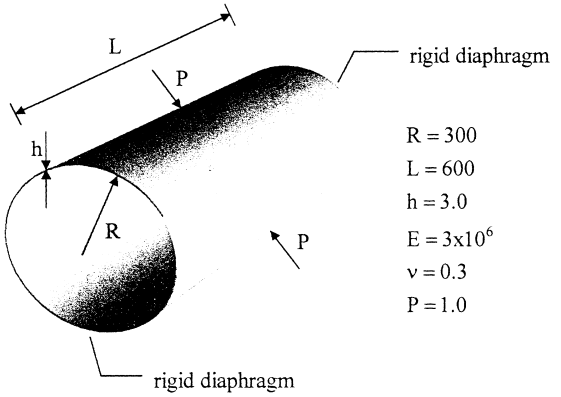

Fig. 14. Material and geometrical data of pinched cylinder.

with respect to the analytical solution ($w^{\text{ref}} = 1.8245\times10^{-5}$) is compared to other solutions extracted from the literature for 4-node quadrilateral elements. Due to symmetry, only one octant of the cylinder is discretized.

4.6. Scordelis-Lo roof

The Scordelis-Lo roof [19] has also achieved the status of a de facto standard test, appearing numerous times in the literature. Depicted in Fig. 15, it represents a cylindrical roof supported by rigid diaphragms and loaded by its own weight. The material and geometrical data of the problem are shown in Fig. 15. In Table 6, the displacement at the midside of the free edge, normalized with respect to the solution computed

Table 5
Pinched cylinder; comparison of the displacement under the applied load between TRIC and 4-node elements (the displacement is normalized with respect to the analytical solution)

Mesh[a]	SRI [14]	RSDS [15]	MITCA4 [16]	Mixed [17]	QPH [18]	TRIC
4×4	0.373	0.469	0.370	0.399	0.370	0.412
8×8	0.747	0.791	0.740	0.763	0.740	0.779
12×12						0.892
16×16	0.935	0.946	0.930	0.935	0.930	0.936
24×24						0.972
28×28						0.981

[a] Octant cylinder.

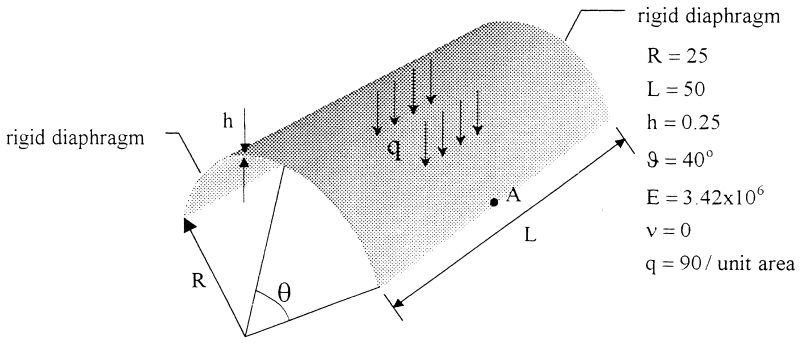

Fig. 15. Material and geometrical data of Scordelis–Lo roof.

by MacNeal and Harder [21] ($w^{\text{ref}} = 0.3024$), is compared to other solutions with 4-node quadrilateral elements. Due to symmetry, only one quarter of the cylindrical roof is discretized.

4.7. Glass-epoxy pressurized shell

This example represents a pressurized orthotropic shell with clamped edges. The problem data are depicted in Fig. 16, while the exact values for the maximum radial displacement $w_{\text{r}}^{\max}$, the central hoop stress $\sigma_{\varphi}^{\text{c}}$ and the central moment M^{c} are given in Rao [20]. Table 7 shows the aforementioned quantities when computed with TRIC element, normalized with respect to the exact values.

4.8. Twisted beam

This particular example deviates from the previous mentioned plate and shell problems. It represents a cantilever beam subjected to a concentrated load applied at the tip in the in-plane direction, as seen in Fig. 17. It is chosen in order to test the effect of warping on plate elements. The undeformed cantilever, as

Table 6
Scordelis-Lo roof: comparison of the displacement at the mid-side of the free edge between TRIC and 4-node elements (the displacement is normalized with respect to the exact solution)

Mesh[a]	SRI [14]	MITCA4 [16]	Mixed [17]	QPH [18]	TRIC
4×4	0.964	0.940	1.083	0.940	0.697
8×8	0.984	0.970	1.015	0.980	0.902
12×12					0.981
14×14					1.001
16×16	0.999	1.000	1.000	1.010	

[a] Quarter cylinder.

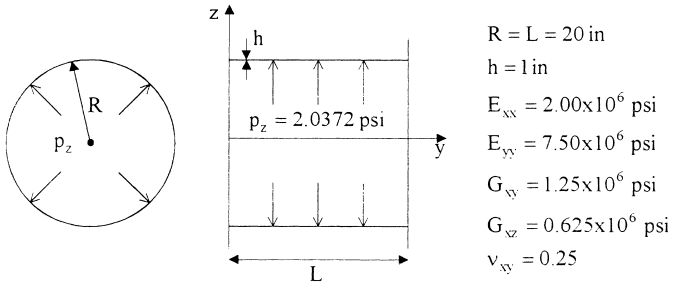

Fig. 16. Material and geometrical data of pressurized cylinder.

Table 7
Glass–epoxy pressurized shell; maximum radial displacement, central hoop stress and central moment normalized with respect to the exact solutions

Mesh[a]	d.o.f.	w_r^{max}	σ_φ^c	M^c
2×2	22	0.667	0.439	0.263
4×4	94	0.928	0.815	0.559
6×6	214	0.989	0.958	0.763
8×8	382	0.996	1.028	0.881

[a] Octant cylinder.

seen in Fig. 17, has a 90° twist, while Table 8 shows the in-plane tip displacement, normalized with respect to the exact solution given by MacNeal and Harder [21] along with the solutions given by other quadrilateral elements.

4.9. Pinched hemispherical shell

The hemispherical shell shown in Fig. 18 is a common doubly curved benchmark example. In the literature it is most often encountered with a hole at the top to avoid the use of triangles near the axis of revolution, when quadrilateral elements are used. For the given, relatively slender, geometry of the shell it is

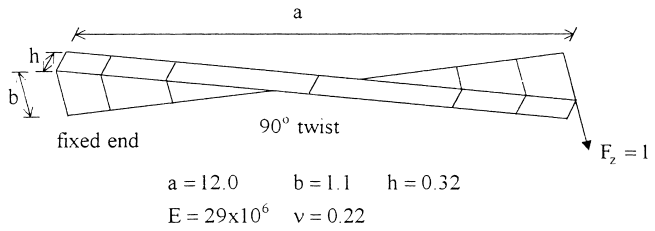

Fig. 17. Material and geometrical data of twisted beam.

Table 8
Twisted beam; comparison of the in-plane tip displacement between TRIC and 4-node elements (the displacement is normalized with respect to the analytical solution)

Mesh	SRI [14]	RSDS [15]	MITCA4 [21]	URI [15]	URI [22]	TRIC
12×2			0.993	1.009	1.004	0.986
14×2						1.007
24×4	0.998	1.411		1.001	0.999	

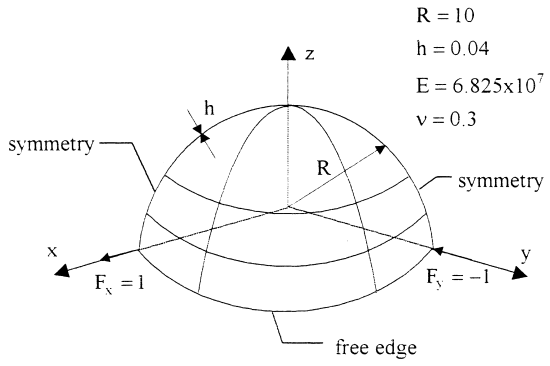

Fig. 18. Material and geometrical data of hemispherical shell.

Table 9
Pinched hemispherical shell; comparison of the displacement under the applied load between TRIC and 4-node elements (the displacement is normalized with respect to the analytical solution)

Mesh[a]	SRI [14]	RSDS [15]	MITCA4 [16]	Mixed [17]	QPH [18]	TRIC
4×4	0.412	0.965	0.390	0.651	0.280	1.022
8×8	0.927	0.971	0.910	0.968	0.860	1.013
12×12						1.003
16×16	0.984	0.989	0.989	0.993	0.990	1.000

[a] Quarter hemisphere.

a small strain, large rotation problem. Large section of this shell under the prescribed load undergoes rigid body rotations. This challenging problem tests the ability of a shell element to represent inextensional bending modes since the membrane strain developing in the thin shell is rather insignificant. In addition, the problem is a test for warping behaviour of shell elements. Only one quarter of the hemispherical shell is discretized, due to symmetry, while in Table 9 the displacement under the applied load, obtained by the TRIC element, is compared to solutions computed by other 4-node quadrilateral elements. The triangular shape of the TRIC element makes it eligible to discretize the hemispherical shell without a hole at the top, while the configuration with the hole at the top is used for the quadrilateral elements. For that reason, the displacement under the applied load calculated with the TRIC shell element is normalized with respect to the theoretical solution ($w^{\text{ref}} = 0.0924$) given by Morley and Morris [23], while the corresponding solutions for the 4-node elements are normalized with respect to the value of 0.0940 given by MacNeal and Harder [21].

4.10. Computational performance

The computational merits of the present formulation are demonstrated by comparing the CPU time required by the TRIC element and by the 8-node serendipity shell element [24] in the case of the clamped isotropic plate of Test 1. The triangular mesh with TRIC elements comprises $20\times20\times2=800$ elements with 2320 degrees of freedom, while the mesh for the 8-node serendipity shell element is 12×12 resulting in 2064 unknowns. Four layers were used in both discretizations. The computations were performed on an SG Power Challenge XL computer. Table 10 shows the time in seconds required for the formation and factorization of the stiffness matrix and the total solution time, for both elements. It can be seen that, for this particular example which represents a linear shell problem, TRIC element performs the computations 7 times faster than the 8-node serendipity shell element using similar number of degrees of freedom for each discretization. This is due to the fact that the computation of the stiffness matrix for TRIC is 40 times faster that the corresponding computation for the isoparametric element. The inexpensive evaluation of the stiffness matrix in the case of TRIC natural mode element is due to its analytical derivation. On the other

Table 10
Comparison of CPU time in seconds between the 8-node serendipity shell element and the TRIC shell element

Type of element	Formulation	Factorization	Total
8-node serendipity	13.6	1.1	15.0
TRIC	0.3	1.1	2.0

hand, the formation of the stiffness matrix for the isoparametric shell element is expensive due to the multiple quadrature loops which are performed.

5. Concluding remarks

In this paper, a more rigorous mathematical foundation for the derivation of the TRIC shell element is presented. By setting TRIC under the light of the non-consistent formulation, it is shown that the proposed element, due to its inherent properties, guarantees convergence to the exact solution. Furthermore, a detailed treatment of the transverse shear deformations is presented in a way that eliminates shear-locking effects. This is demonstrated by showing the analogy of TRIC to the deformations of a beam element assuming that the shell element can be regarded as if it consists of three fictitious beams along the sides of the triangle.

The element's accuracy, robustness and efficiency are tested in a number of standard benchmark plate and shell problems. In both membrane and bending-dominated shell problems, TRIC element exhibits excellent performance. Bearing in mind the computational advantages of the element, due to the analytical derivation of the stiffness matrix, its locking free and shear deformable characteristics as well as its convergence properties, which are demonstrated by showing the intrinsic connection between the non-consistent formulation and the natural mode method, one may conclude that TRIC is a robust element that can be employed in general plate and shell analysis problems.

References

[1] J.H. Argyris, L. Tenek, L. Olofsson, TRIC: a simple but sophisticated 3-node triangular element based on six rigid-body and 12 straining modes for fast computational simulations of arbitrary isotropic and laminated composite shells, Comp. Meth. Appl. Mech. and Eng. 145 (1997) 11–85.
[2] J.H. Argyris, L. Tenek, M. Papadrakakis, C. Apostolopoulou, Postbuckling performance of the TRIC natural mode triangular element for isotropic and laminated composite shells, Comp. Meth. Appl. Mech. and Engrg, 166 (1998) 211–231.
[3] J.H. Argyris, H. Balmer, J.St. Doltsinis, P.C. Dunne, M. Haase, M. Muller, D.W. Scharpf, Finite element method-the natural approach, Comp. Meth. Appl. Mech. and Eng. 17/18 (1979) 1–106.
[4] J.H. Argyris, P.C. Dunne, G.A. Malejanakis, E. Schekle, A simple triangular facet shell element with applications to linear and nonlinear equilibrium and inelastic stability problems, Comp. Meth. Appl. Mech. and Eng. 10 (1977) 371–403.
[5] J.H. Argyris, M. Haase, H.-P. Mlejnek, On an unconventional but natural formation of a stiffness matrix, Comp. Meth. Appl. Mech. and Eng. 22 (1980) 1–22.
[6] J.H. Argyris, L. Tenek, An efficient and locking-free flat anisotropic plate and shell triangular element, Comp. Meth. Appl. Mech. and Eng. 118 (1994) 63–119.
[7] P.G. Bergan, M.K. Nygard, Finite elements with increased freedom in choosing shape functions, Num. Meth. Eng. 20 (1984) 643–663.
[8] P.G. Bergan, L. Hanssen, A new approach for deriving 'good' finite elements, in: Proceedings of the Conference on Mathematics of Finite Elements and Applications, Brunel University, 1975.
[9] P.G. Bergan, Finite elements based on energy orthogonal functions, Num. Meth. Eng. 15 (1980) 1541–1555.
[10] C.A. Felippa, B. Haugen, C. Militello, From the individual element test to finite element templates: evolution of the patch test, Num. Meth. Eng. 38 (1995) 199–239.
[11] M. Braun, M. Bischoff, E. Ramm, Nonlinear shell formulation for complete three-dimensional constistutive laws including composites and laminates, Comput. Mech. 15 (1994) 1–18.
[12] J.N. Reddy, A.K. Pandey, A first-ply failure analysis of composite laminates, Comput. and Struct. 25 (4) (1987) 371–393.
[13] N.J. Pagano, Exact solutions for rectangular bidirectional composites and sandwich plates, Composite Materials 4 (1970) 20–34.
[14] T.J.R. Hughes, W.K. Liu, Nonlinear finite element analysis of shells, part II: two-dimensional shells, Comp. Meth. Appl. Mech. and Eng. 27 (1981) 167–182.

[15] D. Lam, K.K. Liu, E.S. Law, T. Belytschko, Resultant-stress degenerated-shell element, Comp. Meth. Appl. Mech. and Eng. 55 (1986) 259–300.
[16] K.J. Bathe, E.N. Dvorkin, A formulation of general shell elements-the use of mixed interpolation of tensorial components, Num. Meth. Eng. 22 (1986) 697–722.
[17] J.C. Simo, D.D. Fox, On a stress resultant geometrically exact shell element, part II: The linear theory; computational aspects, Comp. Meth. Appl. Mech. and Eng. 73 (1989) 53–92.
[18] T. Belytschko, I. Leviathan, Physical stabilization of the 4-node shell element with one-point quadrature, Comp. Meth. Appl. Mech. and Eng. 113 (1994) 321–350.
[19] A.C. Scordelis, U.S. Lo, Computer analysis of cylindrical shells, Amer. Concr. Inst. 61 (1969) 539–561.
[20] K.P. Rao, A rectangular laminated anisotropic shallow thin shell finite element, Comp. Meth. Appl. Mech. and Eng. 15 (1978) 13–33.
[21] R.H. MacNeal, R.L. Harder, A proposed standard set of problems to test finite element accuracy, Finite Elements in Analysis and Design 1 (1985) 3–20.
[22] B.L. Wong, T. Belytschko, H. Stolarski, Assumed strain stabilization procedure for the 9-node Lagrange shell element, Num. Meth. Eng. 28 (1989) 385–414.
[23] L.S.D. Morley, A.J. Morris, Conflict between finite elements and shell theory, Royal Aircraft Establishment Report, London, 1978.
[24] E. Hinton, D.R.J. Owen, Finite Element Software for Plates and Shells, Pineridge Press, Swansea, UK, 1984.